

Near Infrared and Optical Spectroscopy of FSC10214+4724¹

B. T. Soifer, J. G. Cohen, L. Armus, K. Matthews,
G. Neugebauer and J. B. Oke

Palomar Observatory, Caltech, Pasadena, CA 91125

To appear in: The Astrophysical Journal (Letters)

Received: 1994 October 11; Accepted: 1995 February 3

¹Based on observations obtained at the W. M. Keck Observatory, which is operated jointly by the California Institute of Technology and the University of California

Near Infrared and Optical Spectroscopy of FSC10214+4724¹

B.T. Soifer, J.G. Cohen, L. Armus, K. Matthews, G. Neugebauer, J.B. Oke
Palomar Observatory, Caltech, Pasadena, CA 91125

Received 1994 October 11; accepted 1995 February 3

¹Based on observations obtained at the W.M. Keck Observatory, which is operated jointly by the California Institute of Technology and the University of California

ABSTRACT

New infrared and optical spectroscopic observations, obtained with the W.M. Keck Telescope, are reported for the highly luminous infrared source FSC10214+4724. The rest frame optical spectrum shows new emission lines of [NeIII], [NeV], [OI], [OII], [SII] and He^+ while the rest frame ultraviolet spectrum shows new lines of OIV]+SiIV, NIII, NIV], SiII, NeIV and possibly NII and [NeIII], as well as clearly showing that $\text{L}\alpha$ is self-absorbed. The emission line spectrum is most characteristic of a Seyfert 2 nucleus. The preponderance of spectroscopic evidence strengthens the case for a dust enshrouded AGN powering much or most of the observed luminosity. The various spectral lines lead to a wide range in the inferred reddening and ionization parameter for this system, suggesting that we are viewing several environments through differing extinctions.

Subject headings: Galaxies: Seyfert, Galaxies: Individual - FSC10214+4724

1. Introduction

The IRAS source FSC10214+4724 has been the subject of intensive observational scrutiny since it was found to be at a redshift of 2.286, making it among the most luminous objects in the Universe (Rowan-Robinson, et al 1991). Its prodigious luminosity is matched only by the most luminous quasars. It is likely that an AGN is the main source of power in this object, though star formation probably contributes significantly to the luminosity. The AGN origin of much of the luminosity is suggested by the Seyfert 2 spectral classification (Elston, et al. 1994) and the very large ratio of luminosity to gas mass ($L/M \sim 10^3$ in solar units), while evidence for a significant contribution from star formation comes from the abundant ($10^{11} M_{\odot}$) supply of molecular gas in the system (Brown and Vandebout, 1991, Solomon et al. 1992) and the extended nature of the $H\alpha$ emission (Matthews, et al. 1994).

Complicating the interpretation of this system is the possibility that a nearby companion source, $1.5''$ to the north of the emission line system, could in fact be an intervening galaxy that acts as a gravitational lens (Matthews, et al. 1994, Elston, et al. 1994). This would explain the morphology of the arcs emerging from the emission line source and could explain the elongated and extended nature of the $H\alpha$ source. If the emission-line source is lensed, its intrinsic luminosity would be reduced by a substantial factor from that estimated from its observed infrared flux.

We obtained new infrared and optical spectroscopic observations of both the emission line object (hereafter referred to as the southern source) and the close companion (hereafter referred to as the northern source) in FSC10214+4724 to further probe this most interesting source using the near infrared camera and the low resolution imaging spectrograph on the W.M. Keck Telescope. The new observations reported here add further support to the picture of an AGN origin for the bulk of the observed luminosity, and show that there must be several environments being viewed through different amounts of extinction.

2. Observations and Data Reduction

The infrared observations reported here were obtained on the nights of 1 and 3 May 94 on the W. M. Keck Telescope using the grism mode of the near infrared camera. The instrument, described by Matthews and Soifer (1994), uses a long slit in the focal plane of the telescope, coupled with a grism and bandpass filter. The resolution of the spectrum, with a 0.7" slit width, is $\lambda/\Delta\lambda \sim 80$. The observations were obtained with a 38"x0.7" slit at a position angle of 0 deg, so that both the southern and northern sources (Soifer, et al. 1992) were observed simultaneously. The seeing was $\simeq 0.8''$. Spectra spanning the wavelength ranges 1.0 - 1.6 μm and 1.4 - 2.4 μm were obtained separately. Each set of spectra consisted of a series of observations obtained with the objects at different positions along the slit to facilitate sky subtraction. Individual integrations were 60 or 90 seconds, long enough to be sky background noise limited at all wavelengths. A total of 30 min of integration time was obtained in the 1.0-1.6 μm wavelength range, while 40 min of integration time were obtained on the 1.4-2.4 μm spectrum.

Successive spectral frames were differenced to perform first order sky subtraction. Spectra of the northern and southern sources were then extracted from the difference frames, and the residual sky spectrum was subtracted from the source spectrum in the difference frame. The individual spectra were wavelength calibrated based on spectra of laboratory and astronomical sources, flat fielded and flux calibrated based on spectra of G dwarf stars and then coadded to produce the final spectra of the objects.

The visual observations consisted of spectra obtained on 9-11 March 94 with the Keck Telescope using the low resolution imaging spectrograph (Oke, et al. 1994). Two spectra were obtained, each spanning the wavelength range 0.38 μm - 0.88 μm , with a 300 lines/mm grating and a 1" slit at a position angle of 0 degrees. With a scale of 2.46 \AA /pixel and 5 pixels across the slit in the spectral and spatial domains, the spectral resolution of the

optical spectrum is ~ 750 km/s. The wavelength calibration was obtained from spectra of an argon or neon lamp. The airmass for the spectra was ~ 1.25 . The exposure times were 3000 and 3600 sec. Observations of the standard star GD 248, also taken through a 1" slit, were used to convert the observed spectra of FSC10214+4724 to flux density.

3. Results

The infrared (rest frame optical) spectrum of the southern source in FSC10214+4724, plotted as flux density vs. wavelength, is presented in figure 1. The identified emission lines in the spectrum are indicated in the figure. Table 1 contains the equivalent widths and fluxes of these lines relative to $H\alpha$. None of the (rest frame) optical emission lines were resolved, leading to a limit on the full width at half maximum (FWHM) of $\Delta v \leq 3000$ km/sec. The ratio $[NII]/H\alpha$ was taken from the work of Elston et al (1994).

The rest frame optical spectrum of the southern source is rich in the emission lines expected in AGNs. In agreement with the observations of Soifer, et al. (1991, 1992) and Elston, et al. (1994), the lines of $H\alpha + [NII]$ and $[OIII]$ are seen to be quite strong. The present observations show that other strong lines expected in AGN are also present. All of the strongest lines identified in the spectrum of Cygnus A (Osterbrock, 1989) that are accessible in the atmospheric windows appear to be present in this spectrum. What is most unusual about the observed spectrum is the apparent strength of the rest frame UV lines of $[NeIII]3869\text{\AA}$ and $[NeV]3345,3426\text{\AA}$ and the weakness of the $[OII]3727\text{\AA}$ line.

The low dispersion visual (rest frame UV) spectrum of the southern emission line source is displayed in figure 2. In addition to the strong emission lines of NV , CIV , $HeII$, $CIII]$ and $NeIV$ previously reported by Rowan- Robinson, et al. (1991, 1993) and Elston, et al. (1994), many weaker lines are clearly present. These range from low excitation lines such as NII and $SiII$ to moderate excitation lines such as $OIV]+SiIV$. $Ly\alpha$ is clearly

present, though its peculiar profile and weakness relative to NV are abnormal for AGNs. The profile of Ly α is repeatable in the various spectra obtained, and so is quite reliable. The double peaked profile of Ly α suggests that it is significantly self-absorbed. There is a weak, unidentified line that is blended with CIII]. Table 2 reports the equivalent widths, measured FWHM and fluxes for the identified lines in the rest frame UV spectrum. The FWHM was determined from the best fit single Gaussian to the line profile, and has had the instrumental resolution removed. The widths of the (rest frame) ultraviolet lines are as large as FWHM \sim 1700 km/s, which is greater than values generally associated with Seyfert 2 nuclei.

We obtained spectra of the northern source in the infrared (rest frame optical) and optical (rest frame ultraviolet). These are of significantly lower signal-to-noise ratio than the spectra presented in figures 1 and 2, and no spectral features, either lines or continuum breaks that can confidently be associated with the object are apparent. Weak emission lines at the wavelengths of the observed lines of [OIII] and H α in the southern source are present in the spectrum of the northern source but because these lines are quite bright in the southern source, it is likely that they are simply spillover from the southern source. Thus the present observations cannot address the question of whether the northern source is indeed at the same redshift as the southern source, or is an intervening gravitational lens. With somewhat better seeing, such observations would be quite feasible on the Keck Telescope.

4. Discussion

The rest frame visual/UV spectrum of FSC10214+4724 shows emission lines from a wide range of elements and ionization states, ranging from [OI]6300Å to [NeV]3345Å,3426Å. The detection of the NeV lines demonstrates the presence of 100 eV ionizing photons,

thereby giving strong support to the picture that a substantial fraction of the luminosity in this source originates in a non-stellar source, i.e. an AGN.

The strong far-infrared emission suggests that this source is dusty and possibly heavily obscured, which is consistent with the lack of detection of broad hydrogen recombination lines. This picture of a highly obscured power source is supported by the large $H\alpha/H\beta$ ratio found by Elston, et al. (1994), which suggests $A_v > 5$ mag.

The simple picture of a highly obscured AGN is not, however, consistent with the observations of this source. Qualitatively, the mere detection of the UV lines (Elston, et al. 1994) is inconsistent with the model that the entire emission line region is viewed through > 5 magnitudes of visual extinction. In addition, the observed strong polarization of the rest UV spectrum drops substantially to the rest frame optical (Jannuzi, et al. 1994), suggesting that the UV light is scattered from a polarizing dust cloud, and that different physical regions contribute to the observed spectrum.

The detection of the HeII 4686Å recombination line (figure 1) along with the 1640Å line reported here and by Elston, et al. permits the determination of the reddening between these wavelengths. The observed ratio of the 1640Å and 4686Å lines, ~ 1.3 , corresponds to a reddening $E(1640\text{Å} - 4686\text{Å})$ of 1.8 mag, or a visual extinction of ~ 1.1 mag. The visual extinction inferred from the apparent $Ly\alpha/H\alpha$ line ratio is also 1.5 magnitudes, if an intrinsic line ratio inferred from Case B recombination theory is assumed (Osterbrock, 1989). This is an upper limit to the reddening, since the intrinsic $Ly\alpha/H\alpha$ ratio could be substantially less than that of Case B (Osterbrock).

Further evidence for a multiple component model comes from the line strengths in the observed spectrum. Reddening insensitive emission line flux ratios in the observed spectrum were compared with those calculated using the CLOUDY program (Ferland, 1991) and found to be inconsistent with a single set of model parameters. A series of models were

run with a fixed AGN input ionizing spectrum as characterized by Mathews and Ferland (1987) and Engargiola, et al. (1988). The electron density was varied between 10^2 and 10^6 cm^{-3} , and the ionization parameter (photon flux divided by electron density) was varied from 10^{-4} to 1. For all models the abundances of the elements were assumed to be solar. CLOUDY assumes a plane parallel geometry.

A comparison of the models with the observations of FSC10214+4724 lead us to infer a wide range of extinctions and physical conditions. The predicted line ratios varied little with electron density, but were very sensitive to the ionization parameter. In particular, the observations show strong lines of both low and high ionization, which the models cannot reproduce with a single ionization parameter. The ratios $[\text{NII}]/\text{H}\alpha$ (Elston, et al 1994), and $[\text{OI}]6300\text{\AA}/\text{H}\alpha$ can be matched with ionization parameters in the range 10^{-3} to 10^{-4} , while the ratios $[\text{NeV}]3426\text{\AA}/[\text{NeIII}]3869\text{\AA}$, and $[\text{OII}]3727\text{\AA}/[\text{NeIII}]3869\text{\AA}$ are consistent with ionization parameters of 0.1 - 1. The line ratio $[\text{SII}]6713+6730\text{\AA}/\text{H}\alpha$ is best fit with ionization parameters intermediate between these two sets of values. The line ratio $[\text{OIII}]/\text{H}\beta$, determined by Elston, et al. to be > 64 from the lack of detection of $\text{H}\beta$, cannot be fitted by the CLOUDY models at all. This suggests both strong attenuation of the $\text{H}\beta$ line, and possibly underlying stellar $\text{H}\beta$ absorption. While it is difficult to understand how the higher resolution observations of $\text{H}\beta$ by Elston, et al. might underestimate its strength, the observed spectrum of FSC10214+4724 in figure 1 shows an asymmetric profile of $[\text{OIII}]4959+5007\text{\AA}$, suggesting $\text{H}\beta$ contributes to the blue wing of $[\text{OIII}]$. If this observation is indeed a detection of $\text{H}\beta$, it would be inconsistent with the observations of Elston, et al. but it would be consistent with ionization parameters $> 10^{-2}$.

The observations presented here suggest a picture quite similar to that suggested by Elston, et al. (1994) and Jannuzi, et al. (1994) where the UV spectrum is seen in scattered light, while the optical spectrum is seen directly. In the rest frame wavelengths below $\sim 5000\text{\AA}$ the compact high ionization parameter environment is viewed through a lower

reddening column than is the longer wavelength emission.

The reddening corrected UV flux is not sufficient to directly power the far-infrared luminosity of the source. Correcting the UV/optical continuum for the extinction inferred from the ratio of the He 1640Å and 4686Å lines ($A_v \sim 1.1$ mag) gives a power law continuum spectral index of -0.3. Extrapolating this power-law to the ionization energy of NeV only accounts for $\sim 25\%$ of the infrared luminosity in FSC10214+4724. This fraction is highly uncertain and depends critically on the reddening and the assumption that the power law extends uniformly to ~ 100 eV. If, however, the mean UV flux is affected by greater extinction than determined from the helium lines, or if the observed UV flux is scattered light from a cloud subtending a small solid angle as viewed from the source, or if the mean UV albedo of the reflecting cloud is substantially less than 1, the UV continuum would readily account for the bulk of the infrared luminosity. Alternatively, extrapolating this power-law to X-ray energies can account for the total bolometric luminosity, and remain consistent with the upper limit on the X-ray flux at 3.3 KeV (Lawrence, et al. 1994).

The (rest frame) visual observations are consistent with the picture of the emission lines originating in a large “narrow-line region” more distant from the ionizing source than the gas producing the UV lines. The extended $H\alpha$ source is likely produced in a region even larger than the narrow line region. A low ionization parameter environment is contributing substantially to the observed spectrum at wavelengths longer than 5000 Å. The $[NII]/H\alpha$ and $[OI]/H\alpha$ ratios are inconsistent with stellar ionization (Stasinska, 1990), and lead to substantially lower ionization parameters than the shorter wavelength lines. The line ratio $[SII]/H\alpha$ is consistent with either stellar or non-thermal ionization and an intermediate ionization parameter. The reddening to this region, as determined from the $H\alpha/H\beta$ line ratio is significantly greater than inferred from the UV lines.

5. Summary

Based on the observations of the emission lines, we suggest that the ultimate power source of FSC10214+4724 is a dust enshrouded quasar. The low extinction, high ionization of the UV emission lines coupled with the high extinction, low ionization of the optical emission lines suggests that much of the light below $\sim 5000\text{\AA}$ in the rest frame is reflected through a region of relatively low extinction into our line of sight, while the longer wavelength radiation is viewed directly through higher extinction.

No spectral features are found in the companion object $1.5''$ north of the emission line system. Thus its physical association with the redshift 2.286 system cannot be confirmed.

We would like to thank W. Harrison for assistance with the observations, G. Ferland, Ari Laor and Brian Espey for help in implementing and running the CLOUDY program and Matt Malkan for useful discussions. It is a pleasure to thank the W.M.Keck Foundation and its President, Howard B. Keck, for the generous grant that made the W.M. Keck Observatory possible. Infrared astronomy at Caltech is supported by grants from the NSF and NASA. This research has made use of the NASA/IPAC Extragalactic Database which is operated by the Jet Propulsion Laboratory, Caltech, under contract with NASA.

Table 1: Observed Strengths of Rest Frame Optical Emission Lines

Rest Wavelength	ID	Observed Wavelength	Equivalent Width ^a	R ^b
μm		μm	μm	
0.3346	[Ne V]	1.094	$2.0 \pm 0.6 \times 10^{-2}$	0.36 ± 0.13
0.3426	[Ne V]	1.127	$6.2 \pm 0.6 \times 10^{-2}$	1.17 ± 0.20
0.3727	[O II]	1.232	$3 \pm 2 \times 10^{-3}$	0.07 ± 0.05
0.3869	[Ne III]	1.272	$4.3 \pm 0.3 \times 10^{-2}$	0.88 ± 0.15
0.3967	[Ne III]	1.301	$1.2 \pm 0.3 \times 10^{-2}$	0.25 ± 0.08
0.4072	[S II]+H δ	1.337	$8.5 \pm 3.2 \times 10^{-3}$	0.18 ± 0.07
0.4686	He II	1.541	$9.9 \pm 2.6 \times 10^{-3}$	0.20 ± 0.06
0.4990	[O III]	1.640	$2.0 \pm 0.3 \times 10^{-1}$	4.50 ± 0.64
0.6300	[O I]	2.067	$8.5 \pm 2.3 \times 10^{-3}$	0.14 ± 0.04
0.6562	H α + [N II]	2.149	$1.63 \pm 0.03 \times 10^{-1}$	
	H α		$6.5 \pm 0.9 \times 10^{-2}$	1.00 ± 0.14^c
	[N II]		$9.8 \pm 1.4 \times 10^{-2}$	1.50 ± 0.21^c
0.6724	[S II]	2.202	$8.5 \pm 2.3 \times 10^{-3}$	0.13 ± 0.04
0.7136	[Ar III]	2.330	$5.9 \pm 2.0 \times 10^{-3}$	0.09 ± 0.03
0.7325	[O II]	2.399	$1.4 \pm 0.4 \times 10^{-2}$	0.18 ± 0.06

^aObserved

^bR=F (line)/F(H α)

^cfrom Elston, et al (1994)

Table 2: Observed Strengths of Rest Frame Ultraviolet Emission Lines

Rest Wavelength μm	ID	Observed Wavelength ^a μm	Equivalent Width ^b μm	FWHM ^c km/sec	Flux $10^{-16}\text{erg/cm}^2\text{sec}$
0.1216	Ly α	0.3990	1.00×10^{-2}		11.5 ± 1.7
0.1240	NV	0.4071	1.66×10^{-2}	1740	18.6 ± 2.8
0.1402	OIV]+SiIV	0.4605	5.3×10^{-3}		3.3 ± 0.5
0.1486	NIV]	0.4876	4.8×10^{-3}	1410	3.2 ± 0.5
0.1549	CIV	0.5084	2.45×10^{-2}	1270	15.1 ± 2.2
0.1601	[NeIV]	0.5255	1.6×10^{-3}		0.8 ± 0.3
0.1640	HeII	0.5383	1.24×10^{-2}	890	7.2 ± 1.1
0.1750	NIII	0.5740	2.3×10^{-3}	1480	1.8 ± 0.3
0.1804	SiII+[NeIII] ?	0.5922	1.7×10^{-3}		1.0 ± 0.3
(0.1896)	?	0.6221	1.5×10^{-3}		0.9 ± 0.3
0.1909	CIII]	0.6262	7.1×10^{-3}	965	4.9 ± 0.7
(0.2068)	?	0.6785	1.4×10^{-3}		0.8 ± 0.3
0.2140	NII?	0.7040	1.0×10^{-3}		0.5 ± 0.3
0.2424	NeIV]	0.7953	5.2×10^{-3}	825	3.8 ± 0.6

^auncertainty $\pm 0.0002 \mu\text{m}$

^bobserved width, uncertainty maximum of +3nm,-2nm or 15%

^cuncertainty $\pm 100 \text{ km/sec}$

REFERENCES

- Brown, R.L., and Vanden Bout, P.A. 1991, AJ, 102, 1956.
- Elston, R., McCarthy, P.J., Eisenhardt, P., Dickinson, M., Spinrad, H., Januzzi, B.T., and Maloney, P. 1994, AJ, 107, 910.
- Engargiola, G., Harper, D.A., Elvis, M. and Willner, S.P. 1988 ApJ, 332, L19
- Ferland, G.J. 1991, *OSU Internal Report 91-01*
- Jannuzi, B.T., Elston, R., Schmidt, G.D., Smith, P.S. and Stockman, H.S. 1994, ApJ, 429, L49.
- Lawrence, A., Rigopoulou, D., Rowan-Robinson, M., McMahon, R.G., Broadhurst, T., and Lonsdale, C.J. 1994, MNRAS, 266, L41.
- Mathews, W.G. and Ferland, G.J. 1987, ApJ, 323, 456
- Matthews, K. and Soifer, B.T. 1994, *Infrared Astronomy with Arrays: the Next Generation*, I. McLean ed. (Dordrecht: Kluwer Academic Publishers), p.239
- Matthews, K. et al. 1994, ApJ, 420, L13.
- Oke, J.B., Cohen, J.G. et al. 1994, *SPIE*, 2198, 178
- Osterbrock, D.E. 1989, *Astrophysics of Gaseous Nebulae and Active Galactic Nuclei* (Mill Valley:University Science Books), p. 320.
- Rowan-Robinson, M. et al. 1991, *Nature*, 351, 719.
- Rowan-Robinson, M. et al. 1993, MNRAS, 261, 513.

Soifer, B.T., Neugebauer, G., Matthews, K., Lawrence, C. and Mazzarella, J. 1992, ApJ, 399, L55.

Soifer, B.T. et al. 1991, ApJ, 381, L55

Solomon, P.M., Downes, D., and Radford, S.J.E. 1992, ApJ, 398, L29.

Stasinska, G. 1990, A&AS, 83, 501.

Fig. 1.— The near infrared (rest frame optical) spectrum of the emission line (southern) source in FSC10214+4724. The points represent the flux density per unit wavelength interval plotted vs. wavelength, the thin line represents the uncertainties in the measured flux density, plotted vs. wavelength. The observed wavelengths are plotted along the bottom, while the rest frame wavelenths are plotted on the top. The regions of strong atmospheric opacity are omitted from the plot. All of the strong emission lines are indicated.

Fig. 2.— The optical (rest frame ultraviolet) spectrum of the emission line source in FSC10214+4724. The flux density is plotted vs. wavelength. The observed wavelengths are plotted along the bottom, while the rest frame wavelengths are plotted on the top. The identified emission lines are indicated in the plot.

Normalized Flux Density

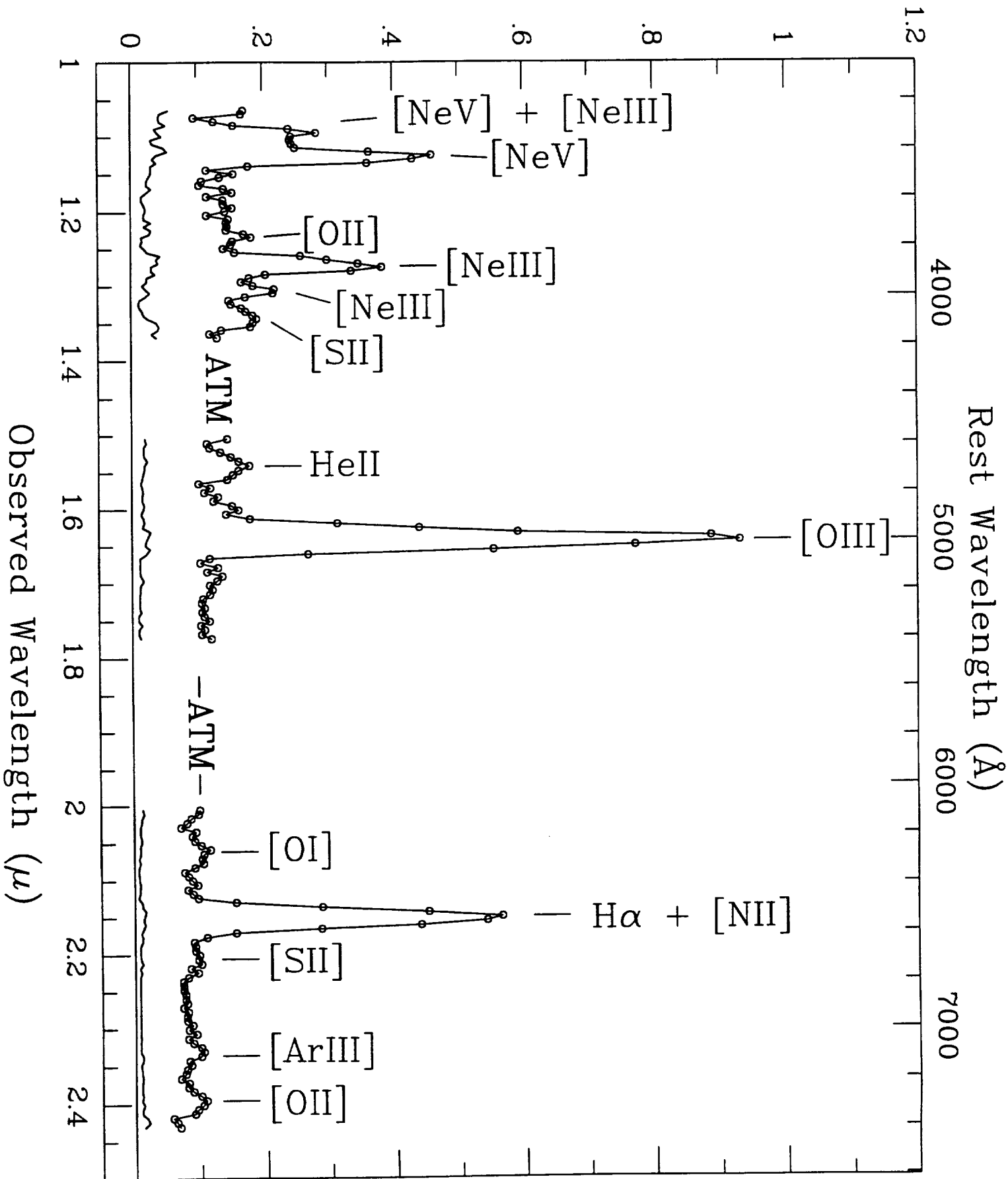


Figure 1

Flux Density (μJy)

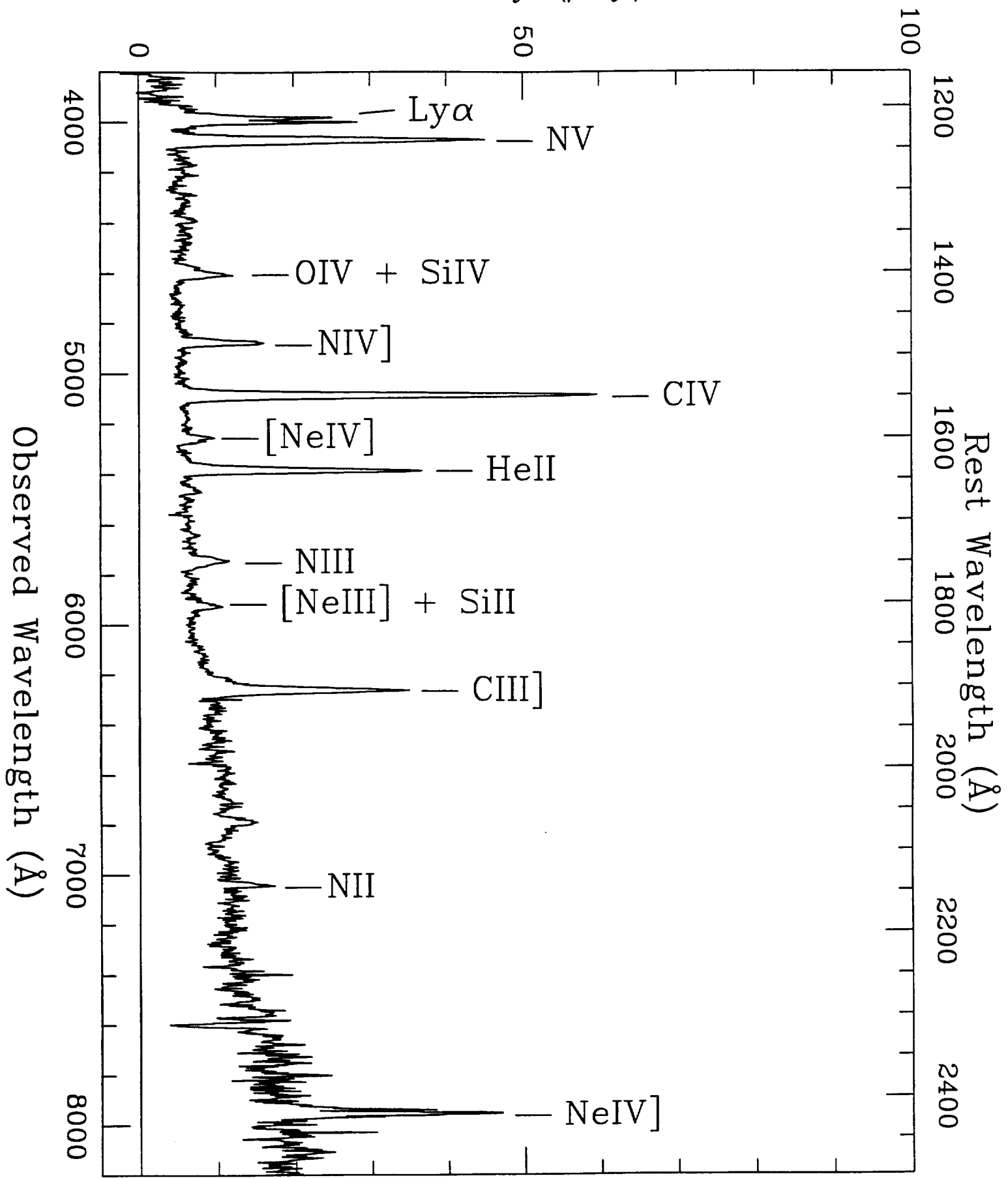


Figure 2

